

Enhanced triethylamine sensing properties by designing Au@SnO₂/ZnO nanosheets directly on alumina tubes

Huanqin Yu, Hongyan Xu*, Wenru Li, Ting Zhai, Zhengrun Chen, Jieqiang Wang, Bingqiang Cao*

Materials Research Center for Energy and Photoelectrochemical Conversion, School of Material Science and Engineering, University of Jinan, Jinan 250022, Shandong, China

ARTICLE INFO

Keywords:

Au@SnO₂/ZnO nanosheets
Au@SnO₂ Schottky contact
SnO₂/ZnO n–n heterojunction
TEA gas sensing

ABSTRACT

A triethylamine (TEA) sensor working temperature of 280 °C with high sensitivity and selectivity for TEA gas has been successfully fabricated by building Au@SnO₂/ZnO nanosheets. By introducing a seed layer, ZnO nanosheets have been directly grown on Al₂O₃ tubes with a facile hydrothermal method. The Au@SnO₂/ZnO structure is formed by utilizing DC-sputtering and pulsed laser deposition (PLD) methods. Compared with the pristine ZnO and SnO₂/ZnO nanosheets sensors, the Au@SnO₂/ZnO nanosheets sensors measured at 280 °C get a higher response of 48.1 toward 50 ppm of TEA gas. Moreover, the Au@SnO₂/ZnO nanosheets sensor exhibits excellent selectivity. The enhanced sensing properties of the Au@SnO₂/ZnO nanosheets are discussed with a model of semiconductor depletion layer on the basis of n–n heterojunction and Schottky contact.

1. Introduction

Triethylamine (TEA), as a significant raw material in industrial and manufacturing areas, is also an effective indicator for assessment of freshness of fish and marine life as it was released from dead fishes and seafoods [1]. However, TEA exerts serious negative influences on human body and environment due to its highly toxic. TEA's threshold limit of concentration in the air is 10 ppm on a volumetric basis (ppmV) [2]. As a result, realizing the rapid, online, trace detection of TEA is of great importance. Thus, it is of great urgency to develop a fast, on-line TEA sensor with high sensitivity and selectivity [3].

Up to now, the metal oxide semiconductor used to detect TEA gas includes ZnO [4] SnO₂ [5,6], α-MoO₃ [7], V₂O₅ [8], WO₃ [9] nanostructures. ZnO is an n-type metal oxide semiconductor with wide band gap energy of 3.37 eV at room temperature and a great exciton binding energy of 60 meV [10–12]. It is one of the widely researched materials with plentiful applications due to its important potential applications, and it shows high electron mobility, good chemical stability [13–15], such as gas sensors [16], nanolasers [17], light emitting diodes [18], etc. Previous reports have suggested that ZnO, especially for the nanostructure ZnO, reveals fine response characteristics to numerous gases such as H₂S [10], butanol [19], acetaldehyde [20] and NH₃ [21].

As we all know, one-dimensional (1D) ZnO nanostructures have some advantages such as high surface to volume ratio, excellent chemical and thermal stabilities, however, the materials' resistance was increased when they formed arrays. By contrast, two-dimensional (2D)

nanostructures such as ZnO nanoplates [16] and nanosheets [22] can overcome the above disadvantages. Rui et al. [23] synthesized the ZnO nanosheets to detect H₂O₂ via electrodeposition. Because of its hexagonal polar structure, the 2D ZnO nanostructure relative to 1D nanostructure is more difficult to grow. Lately, Zeng et al. [22] synthesized ZnO nanosheets thin films with a porous nanostructure by a facile method and reported their CO response, which get the response of 11.2 to 100 ppm gas at 300 °C. In general, ZnO gas sensor can achieve a relative response to target gases only at high temperatures of 300–400 °C. However, these will no doubt lead to high power consumption even may result in ignition of flammable and explosive gases. Therefore, it is meaningful to improve the response and reduce the optimum operating temperature of a gas sensor.

To solve these problems, a number of ZnO-based nanocomposites have been investigated, Fu et al. [24] manufactured two-dimensional net-like SnO₂/ZnO heteronanostructures to detect H₂S, and the enhanced response which compared with the pure SnO₂ and net-like ZnO nanostructures was also demonstrated. Jin et al. [25] fabricated Ga₂O₃-core/ZnO shell nanorod sensors to detect NO₂, when the concentration of NO₂ is 100 ppm, the response value of Ga₂O₃-core/ZnO shell nanorod sensors is 692 times larger than that of bare-Ga₂O₃ nanorod sensors. Lin et al. [26] prepared the TiO₂/ZnO double-layer film sensor, compared with TiO₂ or ZnO film single-layer film, which showed enhanced response toward the NO gas. The noble metals were used to modify the surface of materials which is the other method to the gas-sensing. According to previous research, it is a valid method to improve

* Corresponding authors.

E-mail addresses: mse_xuhy@ujn.edu.cn (H. Xu), mse_caobq@ujn.edu.cn (B. Cao).

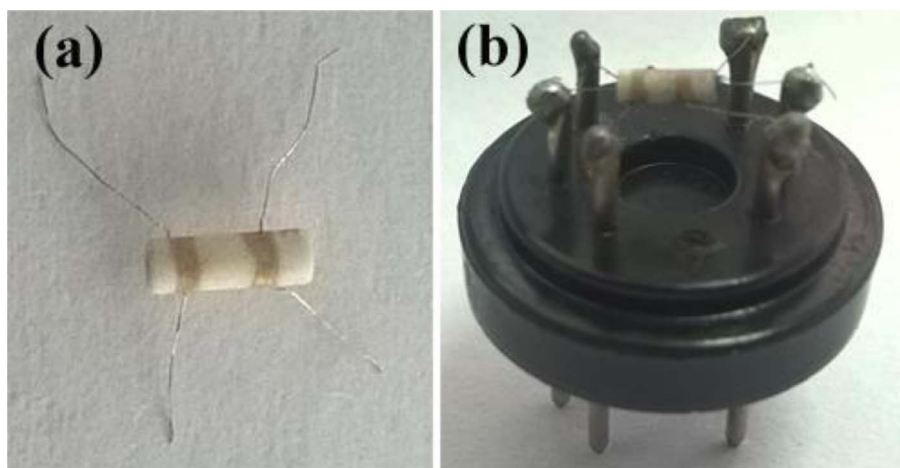


Fig. 1. (a) The image of Al_2O_3 tube; (b) The image of sensor device.

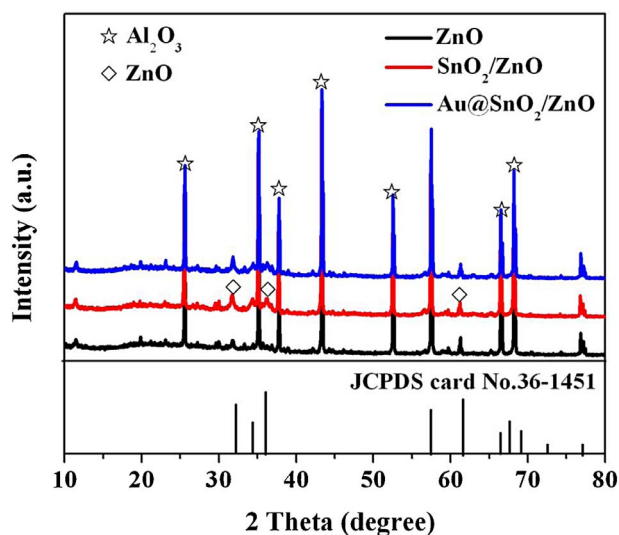


Fig. 2. The XRD spectra of as-synthesized ZnO, SnO_2/ZnO , and $\text{Au@SnO}_2/\text{ZnO}$ nanosheets directly grown on Al_2O_3 substrate.

the gas-sensing properties incorporating the noble with semiconductor oxides by surface modification. Due to the high catalytic activity of noble, the gas-sensing performance can be improved significantly [27–30].

Inspired by the above works, we design and fabricate $\text{Au@SnO}_2/\text{ZnO}$ composite nanosheets on Al_2O_3 tubes to improve the sensing performance of TEA gas on a large scale. The ZnO nanosheets were grown directly on Al_2O_3 tubes using a facile hydrothermal method. SnO_2 as a generally well-known n-type oxide semiconductor with a direct band gap of 3.6 eV [31, 32], is selected to fabricate SnO_2/ZnO n–n heterojunction by PLD (pulsed laser deposition) using SnO_2 target. In addition, the Au@SnO_2 Schottky contacts to be formed by introducing noble metal particles onto the surfaces of SnO_2 nanoparticles. Compared with pure ZnO and SnO_2/ZnO nanosheets, the selectivity and sensitivity of sensors were enhanced markedly after the $\text{Au@SnO}_2/\text{ZnO}$ nanosheets were to be formed. The mechanism of the enhanced sensing properties of $\text{Au@SnO}_2/\text{ZnO}$ nanosheets is discussed in detail in the following sections.

2. Experimental section

2.1. Direct growth of ZnO nanosheets on Al_2O_3 ceramic tubes

In the experiment, all of the chemical reagents we used in this

experiment were purchased from Sinopharm Chemical Reagent (Shanghai, China) and used without further purification. A facile hydrothermal method is used to synthesize ZnO nanosheets [33]. In a typical experiment process as shown below: 0.02 mol $\text{Zn}(\text{Ac})_2 \cdot 2\text{H}_2\text{O}$ was dispersed into 25 ml 2-methoxyethanol. After stirring for 5 h, 1.2 ml ethanolamine was added dropwise into the above solution. We got a clear solution after stirring for 1 h. After 12 h, cleaned Al_2O_3 tubes as shown in Fig. 1(a) (4.0 mm in length, 1.0 mm in internal diameter and 1.4 mm in external diameter) with a pair of Au electrodes (2.0 mm in distance) attached with four Pt wires were immersed into the as-obtained solutions for 8 h and then annealed at 350°C for 30 min to form ZnO seeds layer. Mixed aqueous solution made from zinc nitrate and hexamethylenetetramine was transferred into Teflon-lined stainless steel autoclaves. Meanwhile, the Al_2O_3 tubes were suspended into the aqueous solution. Then we got ZnO nanosheets after the reaction at 95°C for 8 h. Finally, the samples were washed by DI water and ethanol for several times and dried in air.

2.2. Growth of SnO_2/ZnO nanosheets and loading of Au nanoparticles

In this section, the pulsed laser deposition (PLD) was employed to deposit SnO_2 nanoparticles on the surface of ZnO nanosheets. A KrF laser of $1\text{ mJ}/\text{cm}^2$ and an oxygen partial pressure of $3 \times 10^{-4}\text{ Pa}$ were typically applied. The SnO_2/ZnO nanosheet heterojunctions were grown on Al_2O_3 tubes by controlling the laser pulses of 1000 pulses. The experiment process of preparing SnO_2 target as shown below: the mixed powder including 9.0 g SnO_2 powder and 0.1 ml DI water was poured into a mold and spread out, then maintained about 3 min under pressure of 5 MP. After that, the product was dried at 60°C for 6 h. The sintering process was performed in box-type resistance furnace with heating rates of $5^\circ\text{C}/\text{min}$ ($0\text{--}1250^\circ\text{C}$), finally the SnO_2 target with about 25 mm in diameter and 4 mm in thick was obtained. After above mention, Au nanoparticles were loaded onto the surface of SnO_2/ZnO nanosheets by DC-sputtering with a working time of 8 s.

2.3. Material characterizations and sensor properties testing

The morphology, size, composition and crystal structure of obtained samples were checked by scanning electron microscope (SEM, FEI QUANTA FEG250) with an energy dispersive X-ray spectroscopy (EDS, INCA MAX-50), and high-resolution transmission electron microscope (HRTEM, JEM-2100F, JEOL), X-ray diffraction (XRD, D8-Advance, Bruker), and X-ray photoelectron spectrum (XPS) by Al K α -X-ray source (1486.6 eV).

A Ni-Cr resistor, as a heater, was put in the inner of alumina ceramic tube to provide the operating temperature for as-fabricated sensors. The as-fabricated sensors were aged at 340°C for at least 36 h before tests.

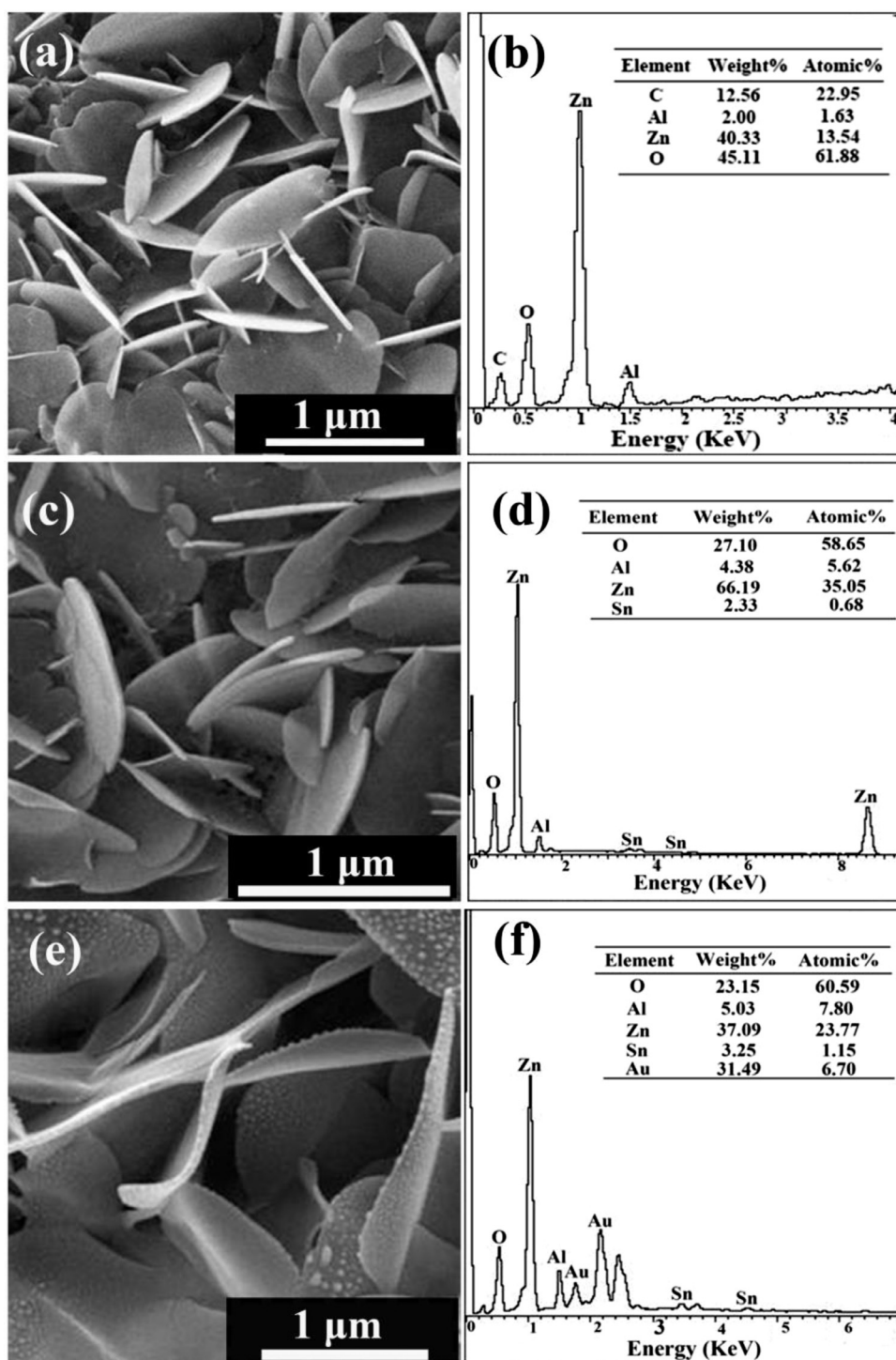


Fig. 3. (a,b) SEM images of ZnO nanosheets directly grown on Al₂O₃ substrate and corresponding EDS spectrum; (c,d) SEM image of SnO₂/ZnO nanosheets and corresponding EDS spectrum; (e,f) SEM image of Au@SnO₂/ZnO nanorod after the implantation of SnO₂ shell and Au nanoparticles and corresponding EDS spectrum.

Therefore, as shown in Fig. 1(b), indirectly-heated sensors have been produced. The gas-sensing properties of sensors were measured with a gas sensing test system (WS-30A, Weisheng Electronics China). A microsyringe was used to inject the gases. The ratio of R_a/R_g was to define the sensor response, where R_a and R_g are the resistances of the sensors in air and in target gas, respectively.

3. Results and discussion

3.1. Characterizations of ZnO, SnO₂/ZnO and Au@SnO₂/ZnO nanosheets

X-ray diffraction analysis was used to study the crystallographic

structure of the obtained samples. XRD spectrum of ZnO, SnO₂/ZnO, and Au@SnO₂/ZnO nanosheets was shown in Fig. 2. It can be observed that part of peaks of as-obtained ZnO nanosheets directly on the Al₂O₃ tube was in good agreement with the JCPDS card 36-1451 and the diffraction peaks of Al₂O₃ substrate are also obvious. The diffraction peaks of Au and SnO₂ of Au@SnO₂/ZnO nanosheets could not be observed owing to their small amount.

The typical SEM image of ZnO nanosheets on the Al₂O₃ tubes is shown in Fig. 3(a), the ZnO nanosheets on the Al₂O₃ tubes stood uniformly and each other was connected to form a network. In order to prove the existence of Zn and O in the above sample, EDS was used to observe the element of the obtained sample. From the EDS spectrum

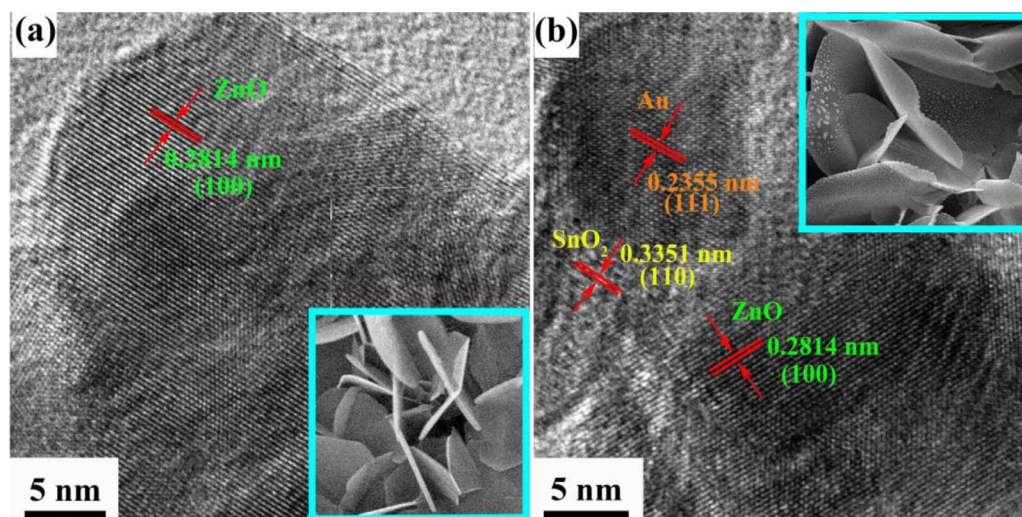


Fig. 4. (a) HRTEM image of ZnO nanosheets; (b) HRTEM image of Au@SnO₂/ZnO nanosheets.

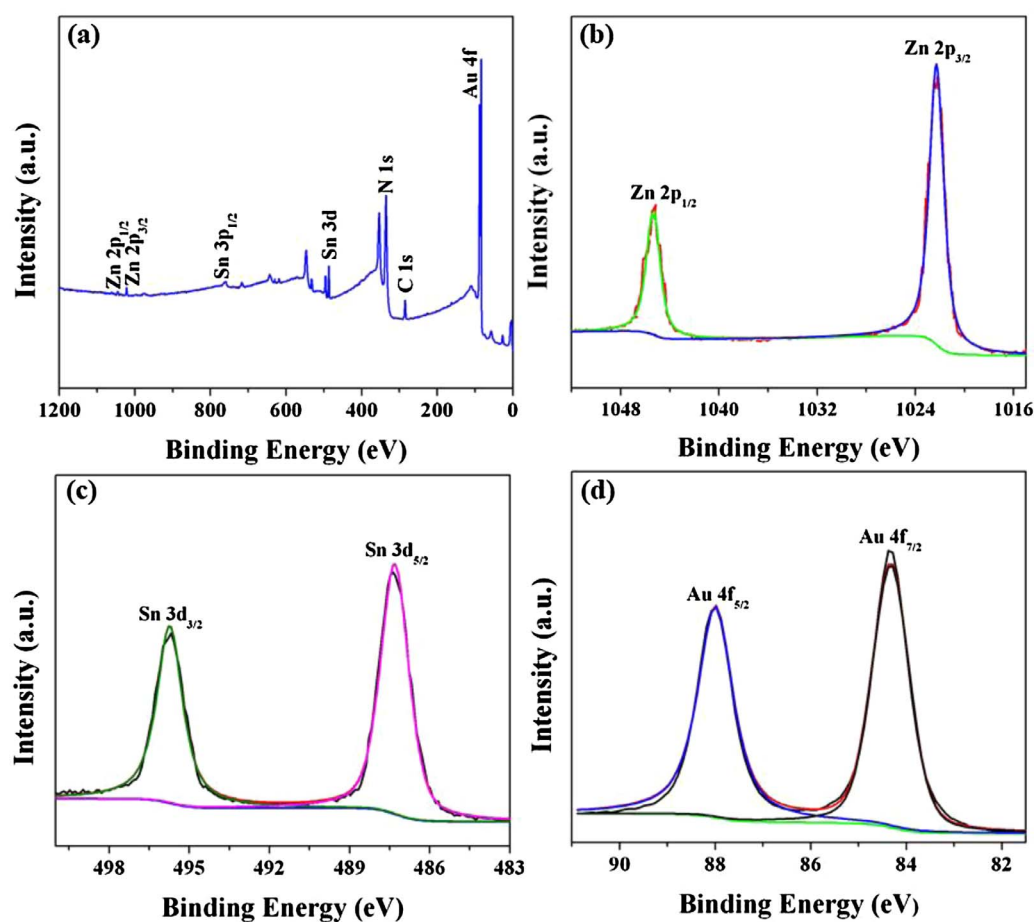


Fig. 5. XPS spectra of the Au@SnO₂/ZnO nanosheets: (a) XPS full survey spectrum; (b) Zn 2p spectrum; (c) Sn 3d spectrum; (d) Au 4f spectrum.

(Fig. 3b) of ZnO nanosheets, we can know that there are two elements in the ZnO nanosheets sample: Zn, O. Due to the conducting resin and Al₂O₃ tubes, there are C and Al elements in this spectrum. In the meantime, there is no the peak of other impurities in the spectrum, indicating that the ZnO nanosheets growing on the Al₂O₃ tubes are pure. Fig. 3(c) and (d) are SEM and EDS images of SnO₂/ZnO nanosheets. The peak of Sn can be seen clearly in the spectrum. And according to the EDS spectrum as shown in Fig. 3(d), the amount of SnO₂ in the SnO₂/ZnO material is about 1.9 mol%. Fig. 3(e) and (f) are SEM and EDS images of Au@SnO₂/ZnO nanosheets. In the Fig. 3(e), the morphology of ZnO nanosheet is preserved after the SnO₂ and Au

nanoparticles were deposited on the surface, and the peak of Au can be seen clearly in Fig. 3(f). And according to the EDS spectrum, the amount of Au and SnO₂ in Au@SnO₂/ZnO material is about 21.19 mol % and 3.64 mol%, respectively.

The HRTEM analysis is used to further investigate the lattice fringes of the ZnO and Au@SnO₂/ZnO nanosheets. The Fig. 4(a) shows the HRTEM image of ZnO nanosheets, the spacing of lattice fringes is about 0.2814 nm, corresponding to the (100) plane of ZnO. Fig. 4(b) shows the HRTEM image of the nanocomposite, the interplanar spacing shown in the image is about 0.3351 nm and 0.2355 nm, corresponding to (110) plane of SnO₂ and (111) plane of Au, respectively. As a result, this

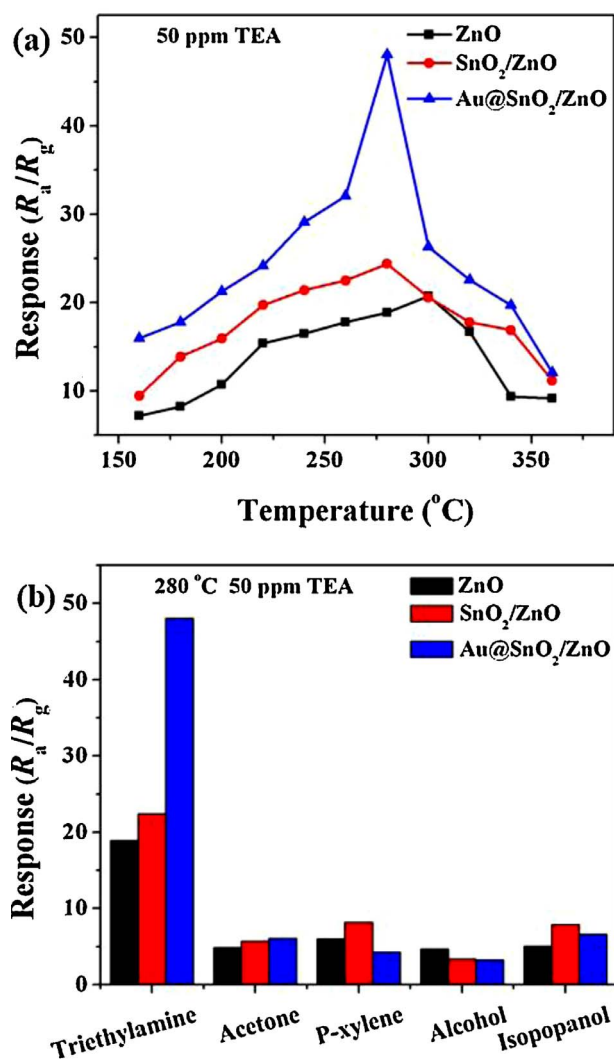


Fig. 6. (a) The relationship between the response and working temperature of sensor 50 ppm TEA gas; (b) Selectivity comparison of three sensors for different target gases at 280 °C.

further confirms that the Au@SnO₂/ZnO nanosheets can be synthesized triumphantly by the present method.

To further check the composition and structure of the surface of the obtained Au@SnO₂/ZnO nanosheets, XPS was performed for Zn, Sn, Au nucleus. Fig. 5(a) shows XPS full survey spectrum, which can be observed obviously the peaks of Zn, Sn, Au, C, and O elements. It might be the reason for the presence of N and C that nitrogen compounds and hydrocarbons have been generated in the synthesis processes of ZnO nanosheets. The decomposition of the Zn 2p peaks displays two components (Fig. 5b), the values of Zn 2p_{3/2} = 1022.18 eV and Zn 2p_{1/2} = 1045.14 eV. As shown in Fig. 5(c), the peaks of Sn element are situated at 487.38 and 495.68 eV, which are ascribed to the Sn 3d_{5/2} and Sn 3d_{3/2}. The peaks of Au are shown in the Fig. 5(d) with the binding energy values of Au 4f_{7/2} = 84.33 eV and Au 4f_{5/2} = 87.98 eV.

3.2. Sensing properties of the ZnO-based nanosheets

For gas-sensing performances of obtained sensors, firstly, the properties of the sensors were measured at various operating temperature, Fig. 6(a) shows the response of ZnO-based nanosheets sensors to 50 ppm TEA at a working temperature from 160 to 360 °C. The optimal operating temperature of Au@SnO₂/ZnO and SnO₂/ZnO sensors is around 280 °C, when the temperature is up to 280 °C, the Au@SnO₂/

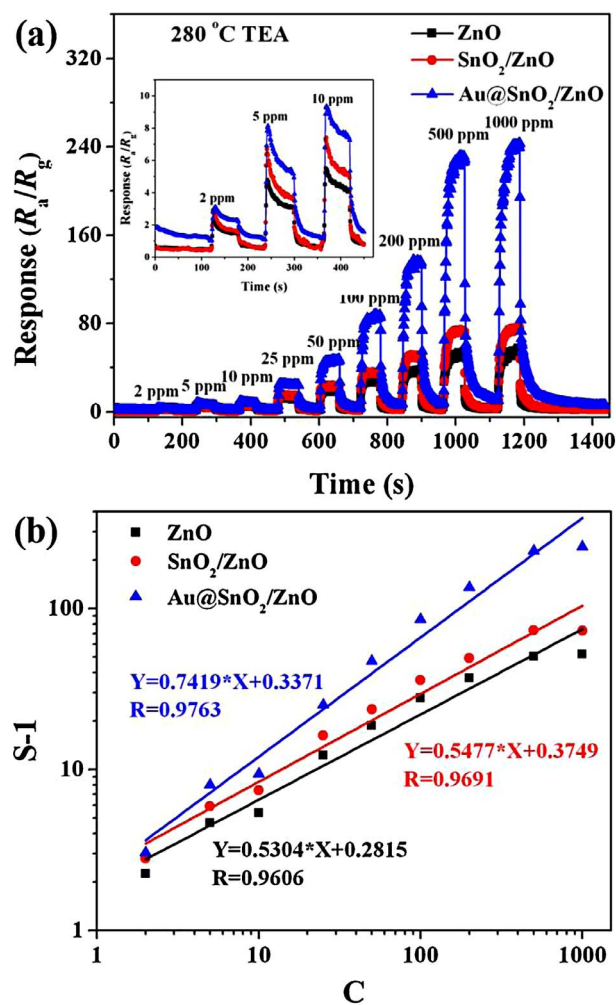


Fig. 7. (a) Response and recovery curves of three kinds of sensors to TEA gas of different concentrations at 280 °C; (b) Linear relationship of log(S-1) versus (C) plot to TEA gas at various concentrations.

ZnO and SnO₂/ZnO sensors exhibit the maximum response of 48.1 and 22.4, respectively. The ZnO nanosheets sensor exhibits the maximum response about 20.7 at around 300 °C. Furthermore, as the working temperature rises, the response decreases, the competing desorption of the chemisorbed oxygen on the surface of the materials might be a reason. Fig. 6(b) shows the ability to select the sensors based on the ZnO nanosheets which are tested with various gases at 280 °C. It can be found that Au@SnO₂/ZnO nanosheets sensors display best selectivity to TEA than ZnO and SnO₂/ZnO sensors. The SnO₂/ZnO n-n heterojunction model in terms of depletion layer and modulation of potential barrier height and Au@SnO₂ Schottky contact might be a reason for selectivity. On the other hand, the different reactivity of target gases according to bond energy may be a possible reason. The primary bond energies of target gases, for example, TEA (C-N), 2-propanol (C-C), ethanol (O-H), and acetone (C=O), are 307, 345, 458.8, and 798.9 kJ/mol, respectively [34].

As shown in Fig. 7(a), at the optimal working temperature, the response curve of obtained sensors of various TEA concentrations from 2 to 1000 ppm was discussed. As a result, Au@SnO₂/ZnO nanosheets sensor exhibits the highest response around the range of 2–1000 ppm TEA, the sensor measured at 280 °C gets a response of 48.1 toward 50 ppm TEA gas, which is about 2.56 times higher than that of the ZnO nanosheet sensor (18.89 for 100 ppm TEA gas). Fig. 7(b) shows the linear relationship of (S-1)-(C) plot to TEA, $S = a[C]^b + 1$ can represent the relationship of response of ZnO-based sensor and

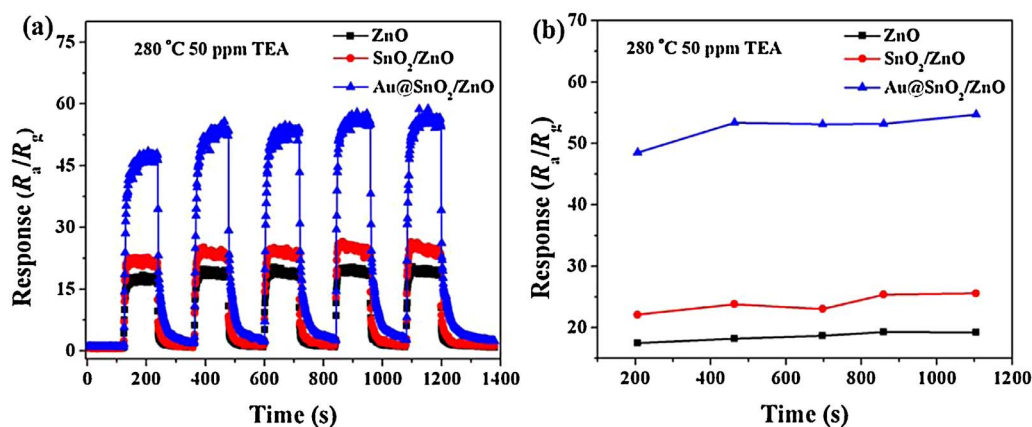


Fig. 8. (a) Repeatability test of the sensors to 50 ppm of TEA at 280 °C; (b) Long-term of the obtained sensors to 50 ppm TEA.

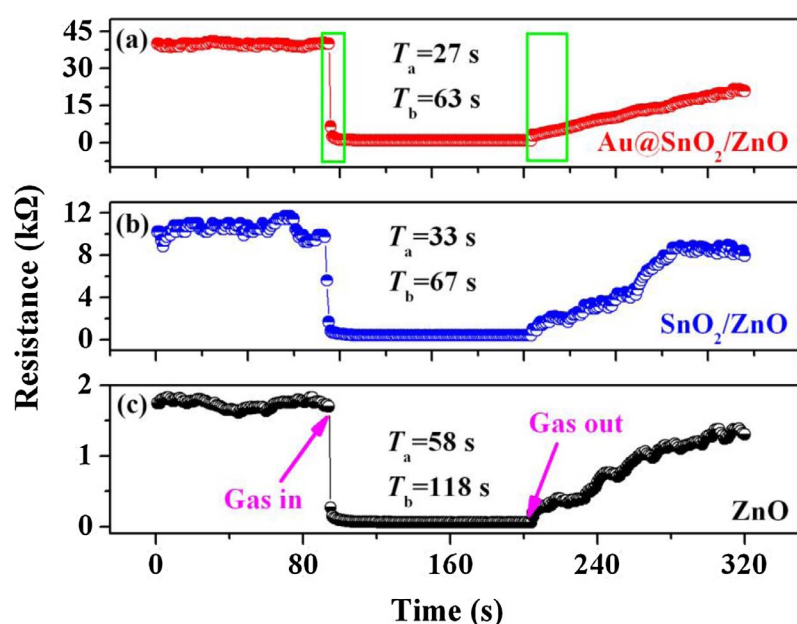


Fig. 9. Response and recovery time of three sensors: (a) Au@SnO₂/ZnO nanosheet sensor; (b) SnO₂/ZnO nanosheet sensor; (c) ZnO nanosheet sensor.

concentration of TEA gas. For $S = a[C]^b + 1$, a and b are the constants, S is the response of ZnO-based sensor, C is the concentration of TEA gas. From the image we can see that pure ZnO, SnO₂/ZnO, and Au@SnO₂/ZnO nanosheets sensors exhibit good linear relationship between the response and concentration in a logarithm scale. The slopes of pure ZnO, SnO₂/ZnO, and Au@SnO₂/ZnO nanosheets sensors are 0.5304, 0.5477 and 0.7419, respectively. It manifests that with the increase of concentration of TEA gas, the response of Au@SnO₂/ZnO nanosheets sensor increases faster than that of pure ZnO, SnO₂/ZnO nanosheets sensors. While three kinds of sensors were measured to 50 ppm of TEA at 280 °C, all sensors exhibit a reproducible run after five cycles as shown in Fig. 8(a) and (b), which proves good device repeatability.

To evaluate the performance of sensors, the response-recovery time is a significant criterion. Fig. 9(a–c) reveals the response and recovery curves of three typical sensors to 50 ppm of TEA at 280 °C. In the Fig. 9(a), the response time of the Au@SnO₂/ZnO sensor is about 27 s.

3.3. Mechanism of the enhanced sensing properties of Au@SnO₂/ZnO nanosheets

The model of space-charge or depletion layer was introduced to demonstrate the basic sensing mechanism of pure ZnO sensors [35–37]. The basic principle of work of oxide semiconductor sensors such as primordial ZnO nanosheets sensors relied on the change of resistance of sensing materials caused by the adsorption and desorption of the target

gas molecules on the surface of the materials. In fact, when the p–n, n–n heterojunctions or metal/semiconductor contacts are formed on the surface of materials, the sensing properties will be enhanced, which has been already reported [25,37–40].

However, the sensing mechanism is still not clear. To our knowledge, the work functions of ZnO, SnO₂, and Au are 5.2, 4.9, and 5.1 eV, respectively [41–43] (Fig. 10a). The n–n junction will be formed after the SnO₂ nanoparticles are applied to the surface of ZnO nanosheet by PLD. Therefore, the electrons of SnO₂ will flow to ZnO until their Fermi energy balances. Because of this, the surface of SnO₂ forms a depletion layer. Beyond that, the energy band was bent and it resulted in a higher resistance state of sensors compared to the pristine ZnO nanosheets (Fig. 10b). Besides, the electrons will flow from SnO₂ to Au nanoparticles when Au nanoparticles are supported on the surface of SnO₂/ZnO nanosheets. This results in the formation of Au@SnO₂ Schottky contact and broadens the depletion layer on the SnO₂. Thus, it continuously increases the materials' resistance of the SnO₂/ZnO nanosheets sensor. Fig. 10(c) shows the energy band graph of Au@SnO₂/ZnO heterojunctions.

Thus, while the Au@SnO₂/ZnO nanosheets were fabricated, because the n–n heterojunction and Schottky contact were formed, the number of electrons of SnO₂ is greatly decreased except the oxygen molecules adsorbed. TEA gas molecules will interact with the preadsorbed oxygen ions when Au@SnO₂/ZnO nanosheets sensors are exposed to the TEA, the electrons further back to Au@SnO₂/ZnO nanosheets. The reaction

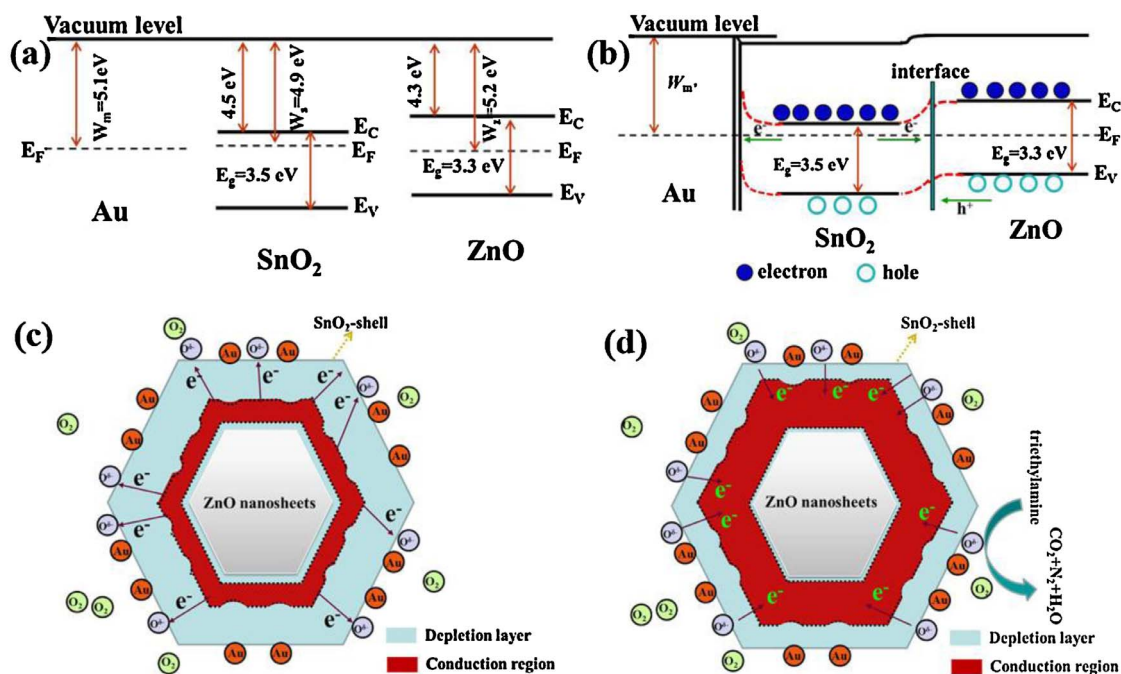


Fig. 10. (a) The energy band diagram of ZnO, SnO₂, and Au; (b) Energy band diagram of Au@SnO₂/ZnO heterojunction; (c,d) Schematic model for the Au@SnO₂/ZnO sensor exposed to air and TEA gas, respectively.

Table 1

TEA sensing properties of Au@SnO₂/ZnO nanosheets and other reported oxide semiconductor sensors working under different operating temperatures.

Material	Concentration (ppm)	Operating temperature (°C)	Response (R _a /R _g)
ZnO nanorods [44]	500	150	300
Porous ZnO foam [45]	90 (ppb)	350	1.4
NiO/ZnO nanosheets [46]	100	320	300
V ₂ O ₅ hollow spheres [47]	100	370	7.3
Cr ₂ O ₃ microspheres [48]	50	170	17
Our works	50	280	48

between TEA gas and oxygen species on the surface of the Au@SnO₂/ZnO nanosheets can be simply depicted as follows:



The height of the barrier due to the Au@SnO₂ Schottky and the width of the depletion layer due to N–N heterojunction were dramatically reduced, leading to a significant decrease in materials resistance, shown in Fig. 10(d). Therefore, according to the sensor response which was defined $S = R_a/R_g$, the enhanced response to TEA is primarily due to the change of resistance caused by the formation of the SnO₂/ZnO heterojunction and Au@SnO₂ Schottky barrier.

Moreover, it may be another reason that the sensitized functions of noble metal particles can further enhance the gas sensing properties of Au@SnO₂/ZnO nanosheets. On the other hand, as an active ingredient, the noble metals can improve the gas-sensing of the sensors. Au nanoparticles are likely to catalyze and accelerate the dispersing speed of oxygen molecules on the surface of the SnO₂, which may also be a reason that leads to the enhanced sensing properties of the Au@SnO₂/ZnO nanosheet. A comparison between the sensing performances of Au@SnO₂/ZnO nanosheet sensors and the TEA gas sensors of literature reported is summarized in Table 1 [44–48].

4. Conclusions

In summary, ZnO nanosheets grew directly on the Al₂O₃ tubes by a facile hydrothermal method. The TEA sensor with high selectivity and sensitivity is formed by designing Au@SnO₂/ZnO nanosheets, and their enhanced sensing mechanism is also discussed in detail. The Au@SnO₂/ZnO nanostructure was formed by using DC sputtering and PLD methods; highly controllable and reproducible are its advantages. The Au@SnO₂/ZnO nanosheets sensors exhibit fast response (~27 s) and high response (48.1) to 50 ppm of TEA gas at the optimum operating temperature of 280 °C, which is much higher than that of pristine ZnO nanosheet sensors and SnO₂/ZnO nanosheets sensors. Compared with pristine ZnO sensors, the resistance of Au@SnO₂/ZnO sensors was increased due to the formation of a depletion layer after the Au@SnO₂ Schottky contact and n–n heterojunction. It is a primary reason for the enhanced gas-sensing properties. Therefore, this study supplies an appropriate way for the enhancement of gas sensing properties of metal oxide semiconductor materials.

Acknowledgements

This work is supported by Shandong Provincial Key Research and Development Program (No. 2017GGX10135), Shandong Provincial Science Foundation (No. ZR2014JL045), and Science Foundation of University of Jinan (No. XKY1504).

References

- [1] S.H. Weng, J.Z. Zhou, Z.H. Lin, Preparation of one-dimensional (1D) polyaniline-polypyrrole coaxial nanofibers and their application in gas sensor, *Synth. Met.* 160 (2010) 1136–1142.
- [2] B. Gandu, K. Sandhya, A.G. Rao, Y.V. Swamy, Gas phase bio-filter for the removal of triethylamine (TEA) from air: microbial diversity analysis with reference to design parameters, *Bioresour. Technol.* 139 (2013) 155–160.
- [3] E. Filippo, D. Mannob, A. Buccolieri, A. Serra, Green synthesis of sucralose-capped silver nanoparticles for fast colorimetric triethylamine detection, *Sens. Actuators B: Chem.* 178 (2013) 1–9.
- [4] S.R. Liu, M.Y. Guan, X.Z. Li, Y. Guo, Light irradiation enhanced triethylamine gas sensing materials based on ZnO/ZnFe₂O₄ composites, *Sens. Actuators B: Chem.* 236 (2016) 350–357.
- [5] H.Y. Xu, D.X. Ju, W.R. Li, J. Zhang, J.Q. Wang, B.Q. Cao, Superior triethylamine-

- sensing properties based on TiO₂/SnO₂ n–n heterojunction nanosheets directly grown on ceramic tubes, *Sens. Actuators B: Chem.* 228 (2016) 634–642.
- [6] H.Y. Xu, D.X. Ju, W.R. Li, H.B. Gong, J. Zhang, J.Q. Wang, B.Q. Cao, Low-working-temperature, fast-response-speed NO₂ sensor with nanoporous-SnO₂/polyaniline double-layered film, *Sens. Actuators B: Chem.* 224 (2016) 654–660.
- [7] S.L. Bai, Y.H. Zhao, J.H. Sun, Z.F. Tong, R.X. Luo, D.Q. Li, A.F. Chen, Preparation of conducting films based on α -MoO₃/PANI hybrids and their sensing properties to triethylamine at room temperature, *Sens. Actuators B: Chem.* 239 (2017) 131–138.
- [8] M.Z. Wu, X.F. Zhang, S. Gao, X.L. Cheng, Z.M. Rong, Y.M. Xu, H. Zhao, L.H. Huo, Construction of monodisperse vanadium pentoxide hollow spheres via a facile route and triethylamine sensing property, *CrystEngComm* 15 (2013) 10123–10131.
- [9] J.H. Sun, X. Shu, Y.L. Tian, Z.F. Tong, S.L. Bai, R.X. Luo, D.Q. Lia, A.F. Chen, Preparation of polypyrrole@WO₃ hybrids with p-n heterojunction and sensing performance to triethylamine at room temperature, *Sens. Actuators B: Chem.* 238 (2017) 510–517.
- [10] J. Kim, K. Yong, Mechanism study of ZnO nanorod bundle sensors for H₂S gas sensing, *J. Phys. Chem. C* 115 (2011) 7218–7224.
- [11] H.Y. Xu, X.Q. Chen, J. Zhang, J.Q. Wang, B.Q. Cao, D.L. Cui, NO₂ gas sensing with SnO₂-ZnO/PANI composite thick film fabricated from porous nanosolid, *Sens. Actuators B: Chem.* 176 (2013) 167–173.
- [12] Y.V. Kaneti, J. Yue, X.C. Jiang, A.B. Yu, Controllable synthesis of ZnO nanoflakes with exposed (1010) for enhanced gas sensing performance, *J. Phys. Chem. C* 117 (2013) 13153–13162.
- [13] C. Soldano, E. Comini, C. Baratto, M. Ferroni, G. Faglia, G. Sberveglieri, Metal oxides mono-dimensional nanostructures for gas sensing and light emission, *J. Am. Ceram. Soc.* 95 (2012) 831–850.
- [14] X.H. Zhang, M.X. Huang, Y.J. Qiao, Synthesis of SnO₂ single layered hollow microspheres and flowerlike nanospheres through a facile template-free hydrothermal method, *Mater. Lett.* 95 (2013) 67–69.
- [15] Z. Qin, Y.H. Huang, J.J. Qi, H. Feng, L.J. Su, Y. Zhang, Facile synthesis and photoelectrochemical performance of the bush-like ZnO nanosheets film, *Solid State Sci.* 14 (2012) 155–158.
- [16] Z.H. Jing, J.H. Zhan, Fabrication and gas-sensing properties of porous ZnO nanoplates, *Adv. Mater.* 20 (2008) 4547–4551.
- [17] J.K. Song, U. Willer, J.M. Szarko, S.R. Leone, S.H. Li, Y.P. Zhao, Ultrafast upconversion probing of lasing dynamics in single ZnO nanowire lasers, *J. Phys. Chem. C* 112 (2008) 1679–1684.
- [18] N. Saito, H. Haneda, T. Sekiguchi, N. Ohashi, I. Sakaguchi, K. Koumoto, Low-temperature fabrication of light-emitting zinc oxide micropatterns using self-assembled monolayers, *Adv. Mater.* 14 (2002) 418–421.
- [19] B.Q. Han, X. Liu, X.X. Xing, N. Chen, X.C. Xiao, S.Y. Liu, Y.D. Wang, A high response butanol gas sensor based on ZnO hollow spheres, *Sens. Actuators B: Chem.* 237 (2016) 423–430.
- [20] G.K. Mani, J.B.B. Rayappan, ZnO nanoarchitectures: ultrahigh sensitive room temperature acetaldehyde sensor, *Sens. Actuators B: Chem.* 223 (2016) 343–351.
- [21] K. Shingange, Z.P. Tshabalala, O.M. Ntwaeaborwa, D.E. Motaung, G.H. Mhlongo, Highly selective NH₃ gas sensor based on Au loaded ZnO nanostructures prepared using microwave-assisted method, *J. Colloid Interface Sci.* 479 (2016) 127–138.
- [22] Y. Zeng, L. Qiao, Y.F. Bing, M. Wen, B. Zou, W.T. Zheng, T. Zhang, G.T. Zou, Development of microstructure CO sensor based on hierarchically porous ZnO nanosheet thin films, *Sens. Actuators B: Chem.* 173 (2012) 897–902.
- [23] Q. Rui, K. Komori, Y. Tian, H.Q. Liu, Y.P. Luo, Y. Sakai, Electrochemical biosensor for the detection of H₂O₂ from living cancer cells based on ZnO nanosheets, *Anal. Chim. Acta* 670 (2010) 57–62.
- [24] D. Fu, C. Zhu, X. Zhang, C. Li, Y. Chen, Two-dimensional net-like SnO₂/ZnO heterostructures for high-performance H₂S gas sensor, *J. Mater. Chem. A* 4 (4) (2016) 1390–1398.
- [25] C. Jin, S. Park, H. Kim, C. Lee, Ultrasensitive multiple networked Ga₂O₃-core/ZnO-shell nanorod gas sensors, *Sens. Actuators B: Chem.* 161 (2012) 223–228.
- [26] C.Y. Lin, J.G. Chen, W.Y. Feng, C.W. Lin, J.W. Huang, J.J. Tunney, K.C. Ho, Using a TiO₂/ZnO double-layer film for improving the sensing performance of ZnO based NO gas sensor, *Sens. Actuators B: Chem.* 157 (2011) 361–367.
- [27] S.Y. Kim, S.H. Park, S.Y. Park, C.M. Lee, Acetone sensing of Au and Pd-decorated WO₃ nanorod sensor, *Sens. Actuators B: Chem.* 209 (2015) 180–185.
- [28] Y.V. Kaneti, J. Moriceau, M.S. Liu, Q. Zakaria, X.C. Jiang, A.B. Yu, Hydrothermal synthesis of ternary α -Fe₂O₃-ZnO-Au nanocomposites with high gas-sensing performance, *Sens. Actuators B: Chem.* 209 (2015) 889–897.
- [29] J. Guo, J. Zhang, M. Zhu, D.X. Ju, H.Y. Xu, B.Q. Cao, High-performance gas sensor based on ZnO nanowires functionalized by Au nanoparticles, *Sens. Actuators B: Chem.* 199 (2014) 339–345.
- [30] S. Vallejos, T. Stoycheva, P. Umek, C. Navio, R. Snyders, C. Bittencourt, E. Llobet, C. Blackman, S. Moniz, X. Correig, Au nanoparticle-functionalised WO₃ nanoneedles and their application in high sensitivity gas sensor devices, *Chem. Commun.* 47 (2011) 565–567.
- [31] B. Cheng, J.M. Russell, W.S. Shi, L. Zhang, E.T. Samulski, Large-scale, solution-phase growth of single-crystalline SnO₂ nanorods, *J. Am. Chem. Soc.* 126 (2004) 5972–5973.
- [32] D.F. Zhang, L.D. Sun, J.L. Yin, C.H. Yan, Low-temperature fabrication of highly crystalline SnO₂ nanorods, *Adv. Mater.* 15 (2003) 1022–1025.
- [33] L.J. Bie, X.N. Yan, J. Yin, Y.Q. Duan, Z.H. Yuan, Nanopillar ZnO gas sensor for hydrogen and ethanol, *Sens. Actuators B: Chem.* 126 (2007) 604–608.
- [34] L.X. Zhang, J.H. Zhao, H.Q. Lu, L. Li, J.F. Zheng, J. Zhang, H. Li, Z.P. Zhu, Highly sensitive and selective dimethylamine sensors based on hierarchical ZnO architectures composed of nanorods and nanosheet assembled microspheres, *Sens. Actuators B: Chem.* 171–172 (2012) 1101–1109.
- [35] T. Gao, T.H. Wang, Synthesis and properties of multipod-shaped ZnO nanorods for gas-sensor applications, *J. Appl. Phys.* 80 (2005) 1451–1454.
- [36] R.K. Sonker, S.R. Sabhajeet, S. Singh, B.C. Yadava, Synthesis of ZnO nanopetals and its application as NO₂ gas sensor, *Mater. Lett.* 152 (2015) 189–191.
- [37] D.M. An, Y. Li, X.X. Lian, Y.L. Zou, G.Z. Deng, Synthesis of porous ZnO structure for gas sensor and photocatalytic applications, *Colloids Surf. A- Physicochem. Eng. Aspects* 447 (2014) 81–87.
- [38] B. Mondala, B. Basumatari, J. Dasb, C. Roychaudhury, H. Saha, N. Mukherjee, ZnO-SnO₂ based composite type gas sensor for selective hydrogen sensing, *Sens. Actuators B: Chem.* 194 (2014) 389–396.
- [39] N.S. Ramgir, P.K. Sharma, N. Datta, M. Kaur, A.K. Debnath, D.K. Aswal, S.K. Gupta, Room temperature H₂S sensor based on Au modified ZnO nanowires, *Sens. Actuators B: Chem.* 186 (2013) 718–726.
- [40] H.C. Chiu, C.S. Yeh, Hydrothermal synthesis of SnO₂ nanoparticles and their gas-sensing of alcohol, *J. Phys. Chem. C* 111 (2007) 7256–7259.
- [41] D.X. Ju, H.Y. Xu, Q. Xu, H.B. Gong, Z.W. Qiu, J. Guo, J. Zhang, B.Q. Cao, High triethylamine-sensing properties of NiO/SnO₂ hollow sphere p-n heterojunction sensors, *Sens. Actuators B: Chem.* 215 (2015) 39–44.
- [42] J. Wang, L. Yu, H. Wang, S. Ruan, J. Li, F. Wu, Preparation and triethylamine sensing properties of Ce doped In₂O₃ nanofibers, *Acta Phys.-Chim. Sin.* 26 (2010) 3101–3105.
- [43] Y. Takao, M. Nakanishi, T. Kawaguchi, Y. Shimizu, M. Egashira, Semiconductor dimethylamine gas sensors with high sensitivity and selectivity, *Sens. Actuators B: Chem.* 24–25 (1995) 375–379.
- [44] Y.Z. Lv, C.R. Li, L. Guo, F.C. Wang, Y. Xu, X.F. Chu, Triethylamine gas sensor based on ZnO nanorods prepared by a simple solution route, *Sens. Actuators B: Chem.* 141 (2009) 85–88.
- [45] J.L. Wang, C.J. Pei, L.J. Cheng, W.P. Wan, Q. Zhao, H.Q. Yang, S.Z. Liu, Responses of three-dimensional porous ZnO foam structures to the trace level of trimethylamine and ethanol, *Sens. Actuators B: Chem.* 223 (2016) 650–657.
- [46] Z.Y. Fan, J.G. Lu, Gate-refreshable nanowire chemical sensors, *Appl. Phys. Lett.* 86 (2015) 123510.
- [47] M.Z. Wu, X.F. Zhang, S. Gao, X.L. Cheng, Z.M. Rong, Y.M. Xu, H. Zhao, L.H. Huo, Construction of monodisperse vanadium pentoxide hollow spheres via a facile route and trimethylamine sensing property, *Cryst. Eng. Commun.* 15 (2013) 10123–10131.
- [48] J. Cao, Y.M. Xu, L.L. Sui, X.F. Zhang, S. Gao, X.L. Cheng, H. Zhao, L.H. Huo, Highly selective low-temperature triethylamine sensor based on Ag/Cr₂O₃ mesoporous microspheres, *Sens. Actuators B: Chem.* 220 (2015) 910–918.